Limnol. Oceanogr., 58(3), 2013, 1008–1022

doi:10.4319/lo.2013.58.3.1008

Environmental selection and resource allocation determine spatial patterns in picophytoplankton cell size

James R. Clark,[1,*] Timothy M. Lenton, Hywel T. P. Williams, and Stuart J. Daines

College of Life and Environmental Sciences, University of Exeter, Exeter, United Kingdom

Abstract

Here we describe a new trait-based model for cellular resource allocation that we use to investigate the relative importance of different drivers for small cell size in phytoplankton. Using the model, we show that increased investment in nonscalable structural components with decreasing cell size leads to a trade-off between cell size, nutrient and light affinity, and growth rate. Within the most extreme nutrient-limited, stratified environments, resource competition theory then predicts a trend toward larger minimum cell size with increasing depth. We demonstrate that this explains observed trends using a marine ecosystem model that represents selection and adaptation of a diverse community defined by traits for cell size and subcellular resource allocation. This framework for linking cellular physiology to environmental selection can be used to investigate the adaptive response of the marine microbial community to environmental conditions and the adaptive value of variations in cellular physiology.

A key challenge facing marine biogeochemical modelers is how best to represent the important role that diverse, rapidly evolving microbial populations play in marine biogeochemical cycles. Simple models, which may include just a single state variable for all phytoplankton (e.g., Fasham et al. 1990), often ignore the distinct functional role that different taxa perform (e.g., silicifying, or calcifying organisms), while more complicated models, which attempt to explicitly resolve multiple functional types (Le Quéré et al. 2005), can face severe practical problems in terms of the number of organism-level measurements and parameters required to describe the model (Anderson 2005; Flynn 2006). A still more fundamental problem lies in how best to represent adaptive or evolutionary processes, which are typically ignored in current state-of-the-art marine ecosystem models.

Recent approaches have attempted to address some of these issues (Follows and Dutkiewicz 2011). For example, Follows et al. (2007) used a Monte-Carlo sampling method with a marine ecosystem model that included a diverse phytoplankton community, described by a set of empirically motivated traits with trade-offs. Emergent patterns in phytoplankton biogeography were in broad agreement with observations, illustrating the importance of environmental selection in determining spatial and temporal patterns in phytoplankton biogeography. The same model has also been used to examine drivers for latitudinal patterns in biodiversity (Barton et al. 2010) and the effect of chromatic adaptation on community structure in oligotrophic environments (Hickman et al. 2010). Meanwhile, Bruggeman and Kooijman (2007) described a biodiversity-based marine ecosystem model in which species were defined by a generic model with continuous trait values for investment in nutrient- and light-harvesting machinery. In their model, trade-offs between traits emerged naturally as a result of different allocation strategies. When configured for a representative oligotrophic open-ocean site, the model was shown to capture several well-known phenomena, including the formation of a deep chlorophyll maximum and nutrient-driven seasonal succession.

These approaches demonstrate the potential of models that include a representation of traits with trade-offs, diversity, ecosystem processes, and environmental selection both to link to ecological and evolutionary theory and to identify the role of different processes in shaping ecosystem structure. Central to a trait-based approach is a representation of diversity and trade-offs between traits, and it is primarily these aspects that we explore here with a new trait-based model. Our overall objective is to take a stepwise approach to constructing a process-based representation of the marine ecosystem that includes adaptation within laboratory-derived physiological constraints. We include a representation of physiology with the aim of identifying the adaptive value of taxa-specific physiological differences. The key elements of the approach are (1) a representation of diversity and trait trade-offs based on a generic cell model with subcellular resource allocation that is grounded in laboratory studies, (2) an agent-based model for environmental interactions of a diverse population that includes individual life histories and evolutionary dynamics, and (3) a bottom-up approach that uses model-data comparisons to identify missing ecosystem processes.

Our overall approach to deriving trait cost-benefit trade-offs from resource allocation and a physiological model for growth as a function of the environment shares many of its design principles with the resource allocation model for terrestrial plants of Tilman (1988, 1990), who investigated questions relating to diversity, resource competition, ecological succession, and environmental selection. The coarse-grained approach to physiology and resource allocation employed here and by Bruggeman and Kooijman (2007)

* Corresponding author: jcl@pml.ac.uk

[1] Present address: Plymouth Marine Laboratory, Plymouth, United Kingdom

is also comparable to the dynamic energy budget approach of Kooijman (2000). The economic analogy for resource allocation and cost-benefit analysis, which is inherent within these different models, was discussed in the context of terrestrial plants by Bloom et al. (1985).

As in Bruggeman and Kooijman (2007), our cell model explicitly resolves the process of allocating resources to different subcellular components—effectively aggregated enzyme systems—and thereby represents the cost benefit of resource allocation as described for phytoplankton by Shuter (1979), Raven (1984), and Geider et al. (2009). In the model, each component functions at an empirically derived rate that, as an initial hypothesis, is assumed to be evolutionarily conserved across taxa. Costs are derived from bottom-up calculations of resource investment (Raven 1994). Biomass generation and growth rate then follow from biophysical constraints (e.g., diffusion limited nutrient uptake), the chain of component rate limitations, and environmental conditions (e.g., light or nutrient availability). To link to laboratory studies of phytoplankton physiology, we build on the work of Shuter (1979) and Geider et al. (1996) while noting that the recent work (Buescher et al. 2012) has also demonstrated the potential of coarse-grained models of subcellular physiology to capture key cost-benefit trade-offs, as determined by detailed omics-based investigations. Importantly, the approach, based on subcellular resource allocation, can represent individual acclimation (as dynamic reallocation to components (Geider et al. 1997; Bonachela et al. 2011), diversity (as constant allocation defined by traits), and adaptation (as changes in allocation through reproduction with variation).

The agent-based modeling approach permits us to track individual life histories and to include evolutionary dynamics (Clark et al. 2011). Each agent represents a clonal population of cells at a point in trait space defined by a digital genome (Clark et al. 2011). Lagrangian agents are then embedded in one-dimensional (1-D) and three-dimensional (3-D) physical environments, defined by the Massachusetts Institute of Technology (MIT) Ocean General Circulation Model (OGCM). Agents grow at a rate determined by environmental conditions and resources and reproduce with variation introduced through random point mutations. Agents may die as a result of predation or by resource starvation. Resources and agents are mixed by the OGCM. The model thus includes resource competition and predator-induced mortality, microevolutionary dynamics, and dispersal.

We thus take a stepwise approach to understanding the role of different processes in shaping ecosystem structure (Thingstad et al. 2010). For this study, allocation is fixed by traits (i.e., acclimation is not represented), and rates of mutation are high, leading to rapid rates of adaptation and effectively a small background input of all species. Thus, the model implicitly includes the assumption that "everything is everywhere" (Baas-Becking 1934), as in Follows et al. (2007) and Bruggeman and Kooijman (2007).

We focus here on controls on cell size, something that was not explicitly considered in the model of subcellular resource allocation presented by Bruggeman and Kooijman (2007). Here, cell size is represented as a trait, where we include two key factors: the effect of size on specific nutrient uptake via diffusion limitation (favoring small cells in nutrient-limited environments; Irwin et al. 2006; Raven 1999) and the cost of this increased nutrient affinity via increased relative resource allocation to cell-surface–associated components in smaller cells. We use a minimal coarse-grained cell model with subcellular components for the photosynthetic apparatus, the biosynthetic apparatus, and cell structure (Fig. 1). For the purpose of this study, which focuses on resource-scarce environments where bottom-up controls on cell size likely dominate (Raven et al. 2005), predation is parameterized by a constant size-independent factor. We therefore omit size-dependent top-down controls favoring investment in defense mechanisms such as armor and (usually) large cell size (Armstrong 1994), which may be important in more dynamic resource-rich environments.

We use this model first to investigate the contribution of bottom-up controls (via nutrient availability and size-dependent nutrient affinity) on community size structure in the global ecosystem and over seasonal times scales at a 1-D time-series site. We then look in more detail at the effect of the light and hence depth-dependent trade-off between nutrient affinity and resource allocation in determining minimum cell size in extreme oligotrophic regions, where competitive exclusion by the smallest cells means that they are dominating the nutrient uptake.

In particular, here we investigate the following questions: What sets the minimum size that organisms inhabiting oligotrophic environments can attain? What costs are associated with extremely small cell size? And how do these factors influence the size structure of microbial communities in these environments? The analysis draws on the work of Raven (1994), who estimated the minimum size limit for prokaryote and eukaryote photoautotrophs by considering the fraction of the cell volume taken up by nonscalable structural components. These include cell membranes, which must maintain a minimum thickness as cell size is reduced, and the minimal amount of genetic material required to encode for all essential ribosomal ribonucleic acids (RNAs), transfer RNAs, and messenger RNAs and thus all essential polypeptides necessary to sustain a free-living photoautotroph. Support for this hypothesis is provided by evidence for the streamlining of both genomes (Giovannoni et al. 2005; Partensky and Garczarek 2010) and cell wall structures (Ting et al. 2007) in the smallest prokaryotes, which imply a selection pressure for minimal architectures and structures in oligotrophic environments and a trade-off between the various benefits associated with small cell size and the necessary allocation of resources to nonscalable components. It is also consistent with the observed larger minimum size for eukaryotes (Raven 1999): the smallest eukaryote *Osterococcus tauri* has an equivalent spherical radius (ESR) of 0.475 μm (Courties et al. 1994) as compared with the smallest prokaryotic photoautotroph *Prochlorococcus*, with an ESR in culture of 0.25–0.35 μm (Morel et al. 1993).

We also draw on recent observations in oligotrophic environments that indicate that the uptake of dissolved inorganic nutrients is dominated by the smallest prokaryotes,

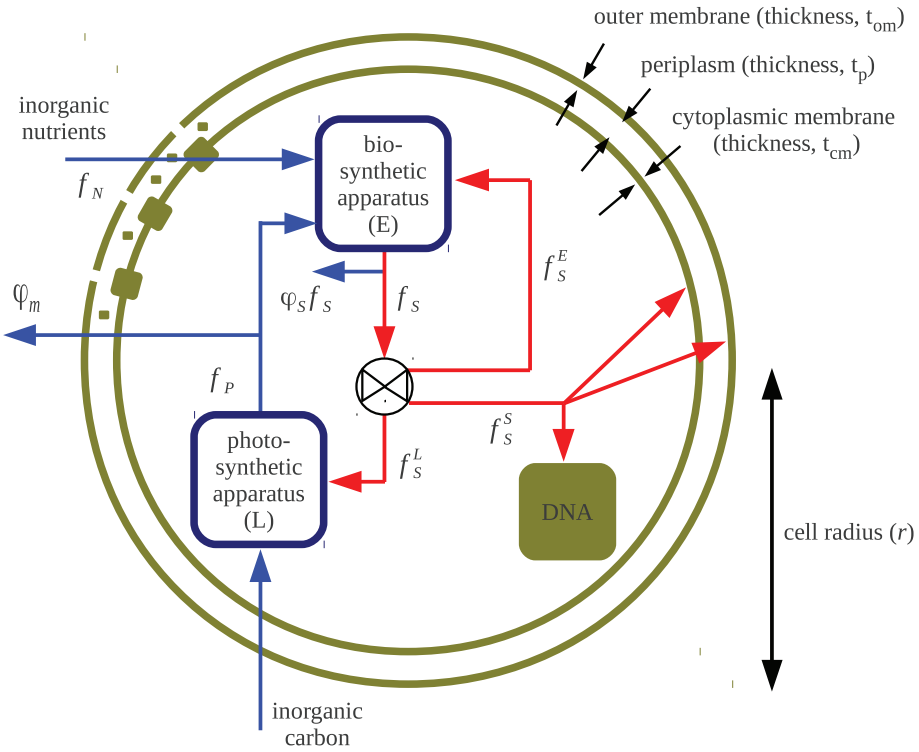

Fig. 1. Model schematic. Solid blue and red arrows indicate specific flow rates, with units h^{-1}. The flows from photosynthesis (f_P) and biosynthesis (f_S) are proportional to the amount of investment in the photosynthetic apparatus and biosynthetic apparatus, respectively. The rate at which diffusion delivers nutrients to the cell (given by f_N) is a function of the cell radius, r. The "control box" (black circle, with valve inset) determines how the products of biosynthesis are allocated to different subcellular components (red arrows). Allocation strategies may be genetically defined, as in the agent-based model (ABM), or derived from optimality principles (*see* main text). Structural material (light brown) consists of genetic material (DNA) and cell surface–associated components, including the cytoplasmic membrane and the outer membrane.

including *Prochlorococcus* and heterotrophic SAR11 (SAR for Sargasso) clade cells (Zubkov et al. 2007), with larger picoeukaryotes appearing to satisfy their nutrient requirements through phagotrophy (Hartmann et al. 2012). These observations are consistent with theoretical models that indicate that smaller cells experience higher diffusion-limited nutrient influxes relative to their requirements for growth in nutrient-limited environments (Chisholm 1992; Kiørboe 2008), which, in steady state, should result in the competitive exclusion of larger organisms, which will tend to have higher limiting nutrient concentrations, as denoted by R^* (Tilman 1982).

The plan for the article is as follows. We first describe the cell model, the bottom-up calculation of size-dependent allocation to structure, and the calculation of optimal allocation in prescribed steady-state environments. We then describe the embedding of the cell model in a trait-based marine ecosystem model in which resource allocation is now determined by traits and is an evolvable property of each population in a diverse phytoplankton community. We then analyze the cell model to derive optimal cell size and resource allocation strategies in steady-state resource-scarce and resource-rich environments. We then use the ecosystem model to first demonstrate that environmental selection for phytoplankton strategies is qualitatively consistent with overall observed trends in biogeography. We then examine trends in cell size with depth in representative oligotrophic environments.

Methods

Cell model—Each cell is divided into three different functional compartments: structural components (S), the photosynthetic apparatus (L), and the biosynthetic apparatus (E; Fig. 1), based on the model of Shuter (1979). These are treated in terms of their fractional contribution to the total cell mass, with the condition that $S + L + E = 1$.

Resource allocation to structural biomass—Resource allocation to "structural" biomass includes all non–light-harvesting and non–biosynthesis-related material and hence represents both nuclear material (deoxyribonucleic acid [DNA]) and cell-surface–associated components (cell surface membranes, including directly membrane-associated proteins, and a less well defined contribution from the periplasm, including binding proteins involved in nutrient transport). This inclusive definition of "cell surface associated" essentially represents a mechanistic approach to quantifying resource allocation to "nutrient uptake machinery," as in Bruggeman and Kooijman (2007). In this

section, we proceed by making a bottom-up calculation based on the inventory of known structural components (DNA and cell membranes), which we would expect to underestimate total allocation to structure, as it ignores the contribution from material within the periplasm (cf. Sowell et al. 2009).

To calculate S, we first make the simplifying assumption that each cell is perfectly spherical (radius, r), and that it possesses a Gram-negative cell wall, meaning that it must allocate resources to an outer membrane and the cytoplasmic membrane. The thicknesses of both the outer membrane and the cytoplasmic membrane, given by t_{om} and t_{cm}, respectively, were assumed to be constant and equal to 8 nm, which is in the middle of the range (6–10 nm) suggested by observations (Neidhardt et al. 1990). The periplasm was assumed to have a thickness (t_{p}) of 15 nm (Madigan and Martinko 2009). The total membrane volume (V_{membs}) is then given by

$$V_{\mathrm{membs}} = \frac{4\pi}{3}\left[\left(r^3 - (r - t_{\mathrm{om}})^3\right) + \left((r - t_{\mathrm{om}} - t_{\mathrm{p}})^3 - (r - t_{\mathrm{om}} - t_{\mathrm{p}} - t_{\mathrm{cm}})^3\right)\right] \quad (1)$$

Membrane density varies depending on the relative fraction of the membrane volume associated with lipids and proteins. Assigning a density of 0.9 and 1.3 Mg m^{-3} to lipids and proteins, respectively, and assuming that the membrane is 70% protein by mass, with the remainder being lipid, yields an overall membrane density, ρ_{membs}, of 1.15 Mg m^{-3} (Raven 1984). The mass of material, m_{membs}, associated with cell membranes is then

$$m_{\mathrm{membs}} = 220 \times \left(\frac{\rho_{\mathrm{membs}}}{1.15\ \mathrm{Mg\ m^{-3}}}\right)\left(\frac{V_{\mathrm{membs}}}{0.19\ \mu\mathrm{m}^3}\right)\mathrm{fg} \quad (2)$$

where we have nondimensionalized the equation using default values for ρ_{membs} and V_{membs} (the latter calculated using a value for r of 1 μm in Eq. 1).

In the case of DNA, which has been observed to scale with cell size (Ting et al. 2007), we simplify the model by focusing on the minimal amount of DNA required to sustain a free-living autotroph. This is achieved by assuming a constant genome size of 1.75 Mbp, equal to that observed in the "near minimal" oxygenic photoautotroph *Prochlorococcus marianus* SS120 (Dufresne et al. 2005). With an assumed mass of 618 Da bp^{-1} (Muddiman et al. 1997), the mass of material associated with DNA (m_{DNA}) is 1.80 fg.

Finally, we assume that the overall cell density, ρ_{cell}, is constant and equal to 1 Mg m^{-3} and that there are 0.47 g dry g^{-1} wet weight (given by $g_{\mathrm{dry\ wt}}$), which is in the middle of the range reported for cyanobacteria (Reynolds 2006). The cell dry mass is then given by the expression

$$m_{\mathrm{cell}} = 480 \times \frac{4\pi}{3}\left(\frac{g_{\mathrm{dry\ wt}}}{0.47\ \mathrm{g\ g^{-1}}}\right)\left(\frac{\rho_{\mathrm{cell}}}{1\ \mathrm{Mg\ m^{-3}}}\right)\left(\frac{r}{1\ \mu\mathrm{m}}\right)^3 \mathrm{fg} \quad (3)$$

where we have again nondimensionalized the equation using default values for different parameters, which yield a cell dry mass of 2000 fg. The fraction of the cell dry mass associated with structural components is then

$$S = \frac{m_{\mathrm{membs}} + m_{\mathrm{DNA}}}{m_{\mathrm{cell}}} \quad (4)$$

Importantly, here allocation to structure is explicitly tied to cell size, which permits us to mechanistically link nutrient acquisition to observations of cell size (c.f. Bruggeman and Kooijman 2007).

Resource allocation and cell growth—Following the necessary allocation of resources to structural components, the remainder, $1 - S$, may be partitioned between the photosynthetic and biosynthetic apparatus without restriction. In the model, L, E, and S are each synthesis products that incur a cost of synthesis, ϕ_{S}, and require nutrient in the fixed stoichiometric ratio, $\omega_{\mathrm{C:P}}$, where phosphate is assumed to be the sole limiting nutrient (*see* Table 1). In addition to a cost of synthesis, all cells pay a maintenance cost, ϕ_m (h^{-1}), which is a function of the ambient temperature, T:

$$\phi_m(T) = \phi_m(T_0)Q_{10}^{(T-T_0)/10} \quad (5)$$

The maximum potential rate of photosynthesis, f_{P} (h^{-1}), is assumed proportional to the investment in light-harvesting machinery L and the light intensity I_z. It is given by the expression

$$f_{\mathrm{P}} = \kappa_{\mathrm{P}} I_Z L \quad (6)$$

where κ_{P} is the efficiency of the photosynthetic apparatus and is empirically derived (Shuter 1979). The products of photosynthesis may be (1) used to satisfy cell maintenance requirements, (2) used for biosynthesis, or (3) wasted (e.g., through fluorescence or nonphotochemical quenching and where we assume that photodamage is negligible).

The actual rate of biosynthesis, f_{S}, is given by the most limiting of three factors: the rate of photosynthesis, the maximum rate of biosynthesis, and the supply of nutrient to the cell (cf. Mei et al. 2009):

$$f_{\mathrm{S}} = \min\begin{cases} \dfrac{(f_{\mathrm{P}} - \phi_{\mathrm{m}})}{1 + \phi_{\mathrm{S}}} \\ \kappa_{\mathrm{S}}(T_0)Q_{10}^{(T-T_0)/10}E \\ f_{\mathrm{N}} \end{cases} \quad (7)$$

The factor $(1 + \phi_{\mathrm{S}})$ accounts for the cost of small and large molecule biosynthesis, expressed as the fractional efficiency in converting carbohydrate to protein, lipid, and other components of biomass. We use the formulation and parameter values of Shuter (1979), which are based on the cost of synthesizing 40% lipid and 60% protein, as taken from Penning De Vries et al. (1974). The maximum rate of biosynthesis is proportional to investment E in the biosynthetic apparatus with (constant) efficiency κ_{S}. The maximum rate of nutrient uptake f_{N} is assumed to be

Table 1. Symbols and units for parameters and variables used in the cell model. Physiological rates are taken directly from Shuter (1979).

Symbol	Value	Units	Description
r		μm	Median cell radius over the division cycle
S		—	Fraction of the cell dry mass associated with structural components
L		—	Fraction of the cell dry mass associated with the photosynthetic apparatus
E		—	Fraction of the cell dry mass associated with the biosynthetic apparatus
μ		h^{-1}	Growth rate
f_P		h^{-1}	Rate of photosynthesis
f_N		h^{-1}	Rate of transfer of nutrient, N, into the cell
f_S		h^{-1}	Rate of transfer of fixed carbon to functional cellular material
f_S^j		h^{-1}	Rate of production of carbon associated with compartment j ($j=S, L, E$)
$\phi_m(T_0)$	0.001	h^{-1}	Cost of maintenance at $T=T_0$
ϕ_S	0.67	—	Cost of synthesis
κ_P	3.9×10^{-3}	$(\mu E\ m^{-2}\ s^{-1})^{-1}\ h^{-1}$	Efficiency of the photosynthetic apparatus
$\kappa_S(T_0)$	0.168	h^{-1}	Efficiency of the biosynthetic apparatus at $T=T_0$
Q_{10}	2		Temperature dependence of biosynthesis and maintenance rates
$\omega_{C:P}$	106		Ratio of carbon to phosphate in functional cellular material
T_0	25	°C	Reference temperature for reaction rates
I_Z		$\mu E\ m^{-2}\ s^{-1}$	Light intensity at depth Z

determined by diffusion to the cell surface (*see* next section).

During active growth, the growth rate, μ, is given by the rate of biosynthesis. During starvation, the growth rate is negative, $f_S = 0$, and $\mu = f_P - \phi_m$:

$$\mu \begin{cases} f_S & \text{if } f_P \geq \phi_m \\ f_P - \phi_m & \text{if } f_P < \phi_m \end{cases} \quad (8)$$

As growth is assumed to be balanced, each separate subcellular component increases (or decreases) in the ratio $L:E:S$.

Nutrient uptake—We assume that the maximum rate of nutrient uptake is diffusion limited and that each cell is a perfect spherical collector, with a nutrient concentration of zero at the cell surface. The maximum per-cell nutrient uptake rate, Q (mol s^{-1}) is then given by (Pasciak 1974; Berg and Purcell 1977)

$$Q = 4\pi D r\ R \quad (9)$$

where D is the molecular diffusion coefficient for a given dissolved nutrient ($\approx 10^{-9}$ m^2 s^{-1} for phosphate) and R is its concentration outside the diffusion boundary layer. Dividing through by the phosphorous content of the cell then gives the mass-specific uptake rate f_N:

$$f_N = \frac{4\pi D r\ R}{\frac{4\pi}{3} \times \frac{1}{12} \times g_{\text{dry wt}} \rho_{\text{cell}} r^3 C_{\text{cell}} \omega_{C:P}^{-1}} \quad (10)$$

where C_{cell} is the fraction of the cell dry mass that is carbon. Nondimensionalizing using default values for the different parameters then gives

$$f_N = 0.060 \times \left(\frac{D}{10^{-9} m^2 s^{-1}}\right) \left(\frac{\rho_{\text{cell}}}{1\ g\ cm^{-3}}\right)^{-1} \left(\frac{g_{\text{dry wt}}}{0.47\ g\ g^{-1}}\right)^{-1} \left(\frac{C_{cell}}{0.5}\right)^{-1} \left(\frac{\omega_{C:P}}{106}\right) \left(\frac{r}{1\ \mu m}\right)^{-2} \left(\frac{R}{1\ nmol\ L^{-1}}\right) h^{-1} \quad (11)$$

As this scales with $1/r^2$ (Kiørboe 2008), smaller cells will naturally possess higher nutrient affinities (Tambi et al. 2009), yielding a significant competitive advantage in nutrient-limited environments.

Optimal allocation in time-independent environments—Optimal cell size and optimal resource allocation to L and E were derived by solving numerically for the maximum growth rate as a function of imposed (and fixed) light and nutrient levels. In cases where the cell size was assumed fixed, optimal values for L and E only were derived. For the fixed cell size case, the graphical approach of Tilman (1982) was used to derive the limiting resource concentration R^* and the corresponding optimal cell size r_{opt} for a given achieved growth rate.

Selection in an ecosystem model—The agent-based model: In the marine ecosystem model, a population of ~ 800 individual Lagrangian agents is maintained in each grid cell of the physical ocean model. Because of computational limitations, we do not model individual cells. Rather, each agent is representative of many identical real-life individuals (Rose 1993; Scheffer et al. 1995). The "split and combine" algorithm of Woods et al. (2005) was applied on a per-grid-cell basis to keep agent numbers within computationally tractable bounds (*see* also Clark et al. 2011). Agents are mixed diffusively in the vertical but for reasons related to computational efficiency are not laterally advected. The vertical diffusion rate used by the circulation model is used to exchange the appropriate fraction of the agent populations between grid cells in each model time step. Accuracy of this agent mixing implementation was verified by comparing the time evolution of the spatial distribution of a set of passive test particles in the agent model with that of tracer transport in the physical model.

The model of subcellular resource allocation was used to determine the growth rate of individual cells, which in turn was used to determine the net uptake (uptake − respiration) of inorganic phosphate by the agent population. Following

Table 2. Symbols and units for parameters and variables used in the evolutionary individual-based marine ecosystem model.

Symbol	Value	Units	Description
m_i		pmol C cell^{-1}	Carbon content of a representative individual belonging to agent *i*
$S_{Sup,i}$		—	Number of representative individuals agent *i* represents
m_0	1	pmol C cell^{-1}	Minimum carbon content of a representative individual
P_{mut}	0.01	% chance per loci	Mutation probability
m_{mort}	0.2	d^{-1}	Effective mortality rate
f_{DOP}	0.67	—	Partitioning of detrital phosphorous between DOP and POP
κ_{DOP}	0.01	d^{-1}	DOP remineralization rate
κ_{POP}	0.033	d^{-1}	POP remineralization rate
ω_{POP}	10	m d^{-1}	POP sinking rate

discretization along the z-axis, this is given by

$$\frac{1}{V_k}\sum_{Agents}\frac{1}{\omega_{C:P}}\mu_i m_i S_{Sup,i} \tag{12}$$

where V_k (m^3) is the volume of the kth depth element, m_i (pmol C cell^{-1}) is the carbon content of an individual belonging to agent i, and $S_{Sup,i}$ is the number of individuals agent i represents (Clark et al. 2011). The rate of change of an individual's carbon content is given by the equation $dm/dt = \mu m$. Individuals reproduce when their carbon content increases from a minimum, m_0, to $m \geq 2m_0$. At the point of division, the parent's biomass is divided between the two offspring, with a small partitioning inequality introduced in order to avoid artifactual synchronization effects (Hellweger and Kianirad 2007).

In the model, mortality is handled stochastically, with agents facing a fixed probability of death each time step, equivalent to a mortality rate, m_{mort}, of 0.20 d^{-1}. At each time step, a virtual coin flip is performed, with the agent killed if this probability is satisfied. When an agent dies, a fraction, f_{DOP}, of the cellular phosphorous is channeled into the dissolved organic phosphorous (DOP) pool, with the remainder released as particulate organic phosphorous (POP). DOP and POP are remineralized back to phosphate at rates κ_{DOP} and κ_{POP}, respectively. POP also sinks through the water column at a rate w_{POP} (m d^{-1}).

Adaptation of genetically defined traits: The method for including genetically defined traits is outlined by Clark et al. (2011). This method uses a genetic algorithm to represent rapid adaptation of the microbial population. Here the model included genetically defined traits for cell size (given by r) and the relative investment in the photosynthetic apparatus (L_{rel}), which determines L through the relationship

$$L = L_{rel}(1 - S) \tag{13}$$

L is thus set by a combination of both L_{rel} and r that directly determines S. E is then calculated using the relationship $S + L + E = 1$.

The term r represents the median cell radius over the cell division cycle—no attempt was made to calculate changes in cell size during an individual's lifetime (i.e., S is calculated from r and considered constant for the lifetime of an individual); r was permitted to vary in the range $0.1 \leq r \leq 2$ μm between individuals, and L_{rel} was permitted to take any value in the range $0 \leq L_{rel} \leq 1$. At the point of reproduction, mutant offspring are created with a probability, P_{mut}. If a mutation occurs on a given trait, a new trait value is selected from a continuous uniform distribution spanning the full range of permissible trait values (i.e., the new trait value associated with the mutant offspring is assumed to be independent of the trait value associated with the ancestor). It should be noted that as the cell radius directly determines S and as S sets the upper bound on L, mutational changes in r, which are independent of L_{rel}, also affect L through Eq. 13.

The physical and biogeochemical model: For global simulations, the evolutionary agent-based marine ecosystem model was coupled to a 2.8° configuration of the MIT OGCM with 15 vertical levels (50 m at the surface, increasing to 690 m at depth), which is briefly described in Adcroft et al. (2011). The model was forced with climatological surface wind stresses (Trenberth et al. 1989) and surface heat and fresh water fluxes (Jiang et al. 1999). Sea surface temperature and salinity were also relaxed toward climatological values (Levitus and Boyer 1994*a,b*). The model includes three passive tracers: dissolved inorganic phosphate (P) as the sole limiting nutrient, dissolved organic phosphorous, and particulate organic phosphorous, which excludes any contribution from living phytoplankton cells.

The rates of change of phosphate, DOP, and POP in the 3-D setup are given by the following equations:

$$\frac{\partial P}{\partial t} + \nabla\cdot(\mathbf{u}P) = \nabla\cdot(K\nabla P) - (\text{uptake} - \text{respiration}) + \kappa_{DOP}DOP + \kappa_{POP}POP \tag{14}$$

$$\frac{\partial DOP}{\partial t} + \nabla\cdot(\mathbf{u}DOP) = \nabla\cdot(K\nabla DOP) - \kappa_{DOP}POP + f_{DOP}\text{Mortality} \tag{15}$$

$$\frac{\partial POP}{\partial t} + \nabla\cdot(\mathbf{u}POP) = \nabla\cdot(K\nabla POP) - \frac{\partial}{\partial z}(w_{POP}POP) - \kappa_{POP}POP + (1 - f_{DOP})\text{Mortality} \tag{16}$$

where $\mathbf{u}$ is the transformed Eulerian mean velocity including a parameterization of mesoscale eddy transport and K is a mixing tensor representing isopycnal and

diapycnal mixing (Gent and McWilliams 1990). Other symbols and parameter values are listed in Table 2. Agents were mixed diffusively in the vertical, as described below for the 1-D configuration, but were not laterally advected. The model was run forward for 5 yr, after which time there remained a small residual drift in globally integrated net primary production (NPP). Annual means were formed for the fifth year of the simulation.

For the 1-D simulation, we used a variable vertical grid consisting of 35 depth levels, with a resolution of 10 m in the top 140 m, 15 m down to 215 m, and steadily increasing thereafter. The model was integrated forward for 20 yr, with results taken from the 20th year of the simulation. The rates of change of phosphate, DOP, and POP in the 1-D setup are given by Eqs. 14–16 but without lateral nutrient advection. The model was configured for the Bermuda Atlantic Time Series (BATS) site (31°50′N, 64°10′W) in the Sargasso Sea. Physical (temperature) and biogeochemical (phosphate) fields were initialized using data from the World Ocean Atlas (WOA) 2005 (Garcia et al. 2006; Locarnini et al. 2006). Salinity was kept uniform throughout the water column at 35.

In the 1-D setup, lateral nutrient advection, which can be important in terms of NPP in the oligotrophic subtropical gyres (Williams and Follows 1998, 2003), was parameterized by imposing a constant lateral nutrient in flow of 4.82×10^{-12} mol P m^{-3} s^{-1} over the top 100 m of the water column. This nutrient source, based on values taken from (Williams and Follows 2003), effectively balances out the loss of nutrient to the main thermocline via the export of organic material below the seasonal boundary layer (Williams and Follows 2003). In order to prevent the excessive buildup of nutrient below the seasonal boundary layer, nutrients were also relaxed toward climatological values using a relaxation time scale of 1 yr.

Vertical mixing rates were calculated using the K-Profile Parameterization scheme of Large et al. (1994). Mixed-layer dynamics were driven by relaxing sea surface temperature toward monthly climatological values from the WOA using a relaxation time scale of 3 d (Hickman et al. 2010). The model was also forced at the surface with monthly climatological wind stresses from Trenberth et al. (1989).

Model evaluation: Depth-integrated NPP for the fifth year of the global simulation was in qualitative agreement with observations in the oligotrophic subtropical gyres, which are the main focus of this study. However, the model overestimates production in high-nutrient, low-chlorophyll regions, such as the equatorial Pacific and regions of the Southern Ocean, in part reflecting the absence of micronutrient limitation in the model. For 1-D simulations, NPP and carbon export at 150 m were within observational bounds at BATS (Karl et al. 2003). The contribution of nutrient entrainment and lateral nutrient advection to new production are ~ 26% and ~ 64%, respectively. The relatively small contribution from nutrient entrainment is likely a result of a somewhat shallow winter mixed layer that extends down to just 180 m, as compared with observations that indicate that winter mixed-layer depths vary between 160 and 300 m on average (Steinberg et al. 2001).

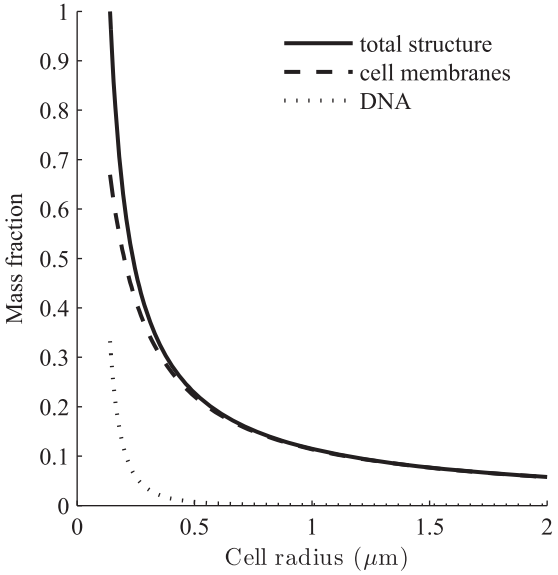

Fig. 2. Fraction of the cell dry mass associated with cell membranes and the genome in a perfectly spherical Gram-negative photoautotroph as a function of the cell radius r. Calculations based on Raven (1994).

Results

Allocation to structure as a function of cell size—The calculated fraction of the biomass taken up by structural components (*see* Methods) is shown in Fig. 2. We find that the fraction of the total dry mass taken up by the near minimal compliment of nonscalable components in a *Prochlorococcus* cell with a cell radius of 0.5 μm is ~ 25%, which is equivalent to ~ 18% of the total cell dry mass being associated with membrane-bound proteins (assuming a constant protein density per membrane area). Our calculation also indicates that structural components constitute a significant ($> 50\%$) fraction of the cell dry mass in spherical Gram-negative photoautotrophic cells with radii $\lessapprox 0.2$ μm. This result is consistent, given the approximate nature of the calculation, with the apparent ~ 0.25 μm lower ESR limit observed for *Prochlorococcus* (Morel et al. 1993), and the observed minimum size of heterotrophic *Pelagibacter ubique* cells, with an ESR of ~ 0.18 μm (Nicastro et al. 2006). It is also consistent with metaproteomic analyses of *P. ubique* that indicate that ~ 80% of proteins are transport related (Sowell et al. 2009), which are logically assigned to structural components.

Optimal cell allocation and size in time-independent environments—For time-independent environments, we can define optimal allocation strategies as those that maximize either growth rate (for the nutrient unlimited case) or competitive ability for resources (for the nutrient-supply–limited case).

Optimal cell size and allocation to L and E: Maximization of growth rate gives the optimal cell size and optimal

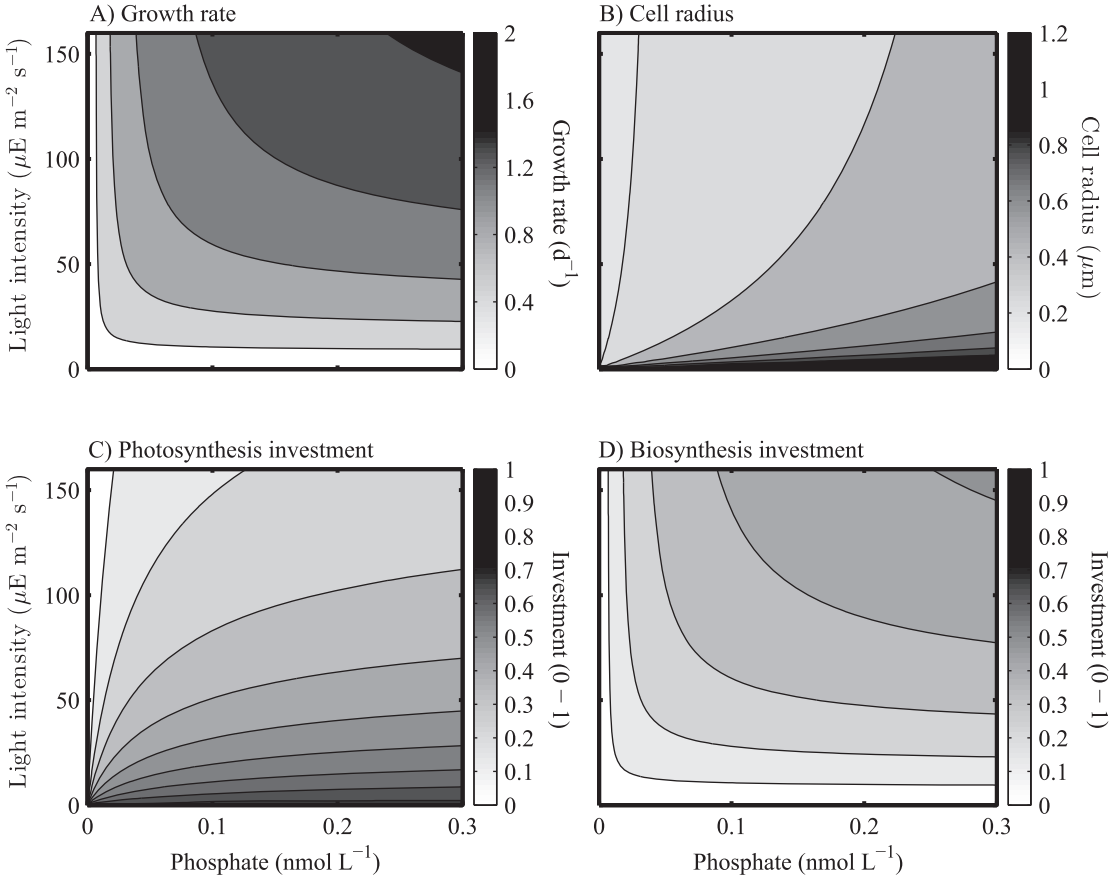

Fig. 3. (A) Achieved growth rate, (B) the optimal cell size, (C) optimal photosynthesis investment, and (D) optimal biosynthesis investment as a function of the external nutrient concentration (horizontal axis) and light level (vertical axis).

allocation to the photosynthetic (e.g., chlorophyll, accessory pigments) and biosynthetic (e.g., ribosomes) machinery for a range of different environmental conditions, as shown in Fig. 3. At a given light intensity, lower nutrient levels favor smaller cells (Fig. 3B), necessarily decreasing the relative allocation to the photosynthetic (Fig. 3C) and biosynthetic (Fig. 3D) machinery through increased allocation to structure. At a given nutrient level, lower light levels favor larger cells, allocating more resources to the photosynthetic machinery, as in Shuter (1979).

Optimal size for competitive ability for resources: For the steady-state, nutrient-supply–limited case (a chemostat or an oligotrophic, permanently stratified, low-latitude marine environment with competitive exclusion by the smallest cells), the optimal cell size and subcellular resource allocation strategy follow from resource competition theory (Tilman 1982). Competition for resources will drive the nutrient concentration down to the lowest limiting nutrient concentration where the population growth rate balances losses (via predation, viral lysis, and so on) from the system and nutrient supply determines the population size.

The achieved (maximized) growth rates for optimally allocating cells grown in high-light and low-light conditions for a range of different resource concentrations and cell sizes are shown in Fig. 4A,B, respectively. For a given set of environmental conditions, there is an optimal cell size that maximizes the organism's growth rate (cf. Fig. 3). For cells below this size, the organism is effectively hampered by the necessary allocation of resources to structural components, reducing its potential biosynthetic and photosynthetic capacity. For cell sizes above this, the growth rate is limited by the rate at which diffusion delivers nutrients to the cell. For a given imposed loss rate, the optimal cell size and R^* can then be derived graphically (Fig. 4A,B) as the point on the zero-net-growth isocline with the smallest cell size and nutrient level. Both R^* and optimal cell size are higher under low-light conditions, reflecting the fact that the organism must allocate more resources to the photosynthetic apparatus.

Environmental controls on cell size in a model ocean: Global biogeography and controls on cell size: When coupled to the 3-D OGCM, environmental selection results in emergent patterns in phytoplankton cell size and allocation strategies (Fig. 5), demonstrating the influence of bottom-up controls and dynamics on phytoplankton biogeography (Irwin et al. 2006; Dutkiewicz et al. 2009). In the model, larger (ESR approximately > 1 μm) fast-growing cells dominate in high-latitude bloom-forming environments (Fig. 5). In these dynamic regions, resource levels are not drawn down to steady-state limiting values, and cell sizes between the minimum and the diffusion-limited maximum are favored. In contrast, smaller (ESR approximately < 0.5 μm) cells dominate in stable

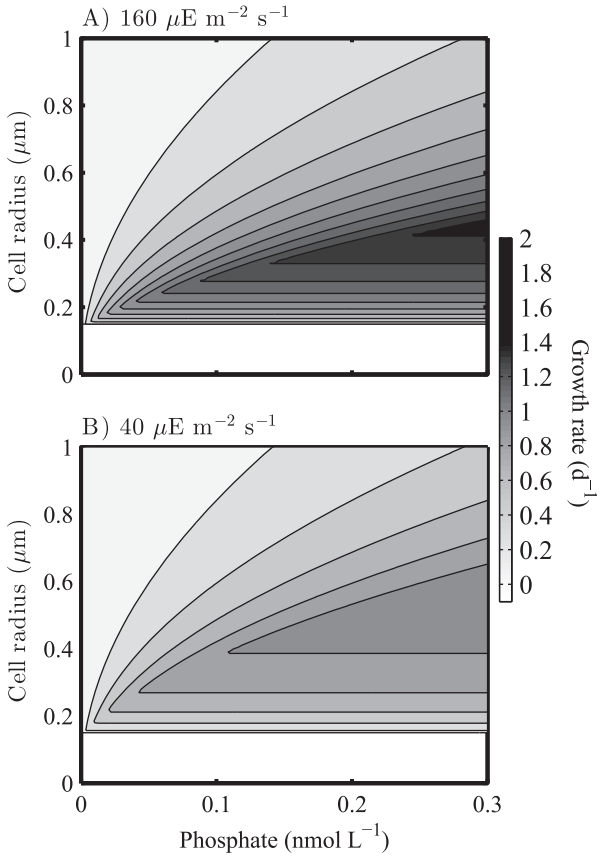

Fig. 4. Achieved growth rate in (A) high- and (B) low-light environments of optimally allocating cells as a function of cell size (vertical axis) and the external nutrient concentration (horizontal axis). In steady-state environments, where losses exactly balance gains, contour lines represent zero-net-growth isoclines. The leftmost points on each contour line give theoretical values for the equilibrium nutrient concentration R^* (horizontal axis) and the optimum cell size r_{opt} (vertical axis). The growth of cells larger than r_{opt} is limited by the diffusive transport of nutrients. Cells smaller than r_{opt} have lower growth rates due to increased structural overheads.

low-latitude oligotrophic environments, where competition for resources results in nutrient drawdown and the competitive exclusion of larger cells.

In the absence of top-down controls, the model underpredicts cell size except in the most extreme oligotrophic regions. Outside of these regions, size-dependent predation will limit the population size of the smallest cells, allowing nutrient levels to rise and larger size classes to persist in both steady-state and dynamic environments (Chisholm 1992; Armstrong 1994). Our model is then most applicable in extreme oligotrophic regions, where the smallest (i.e., *Prochlorococcus*) photoautotrophs dominate autotrophic nutrient uptake, indicating that bottom-up controls on phytoplankton cell size dominate.

Seasonality and bloom dynamics in a 1-D environment: To further investigate the effect of bottom-up controls on cell size and to illustrate the limit of the oligotrophic region within which they likely dominate, we explore trends in the size of phytoplankton cells with changes in light intensity

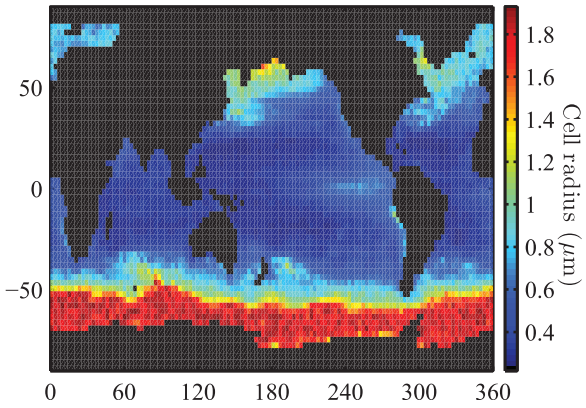

Fig. 5. Modeled annual mean of the biomass-weighted mean population cell size in the top 50 m of the water column for the fifth year of a 5 yr simulation. Small cell sizes in low-latitude, oligotrophic environments identify regions where the trade-off between cell size, nutrient affinity, and growth may help to control the size distribution of phytoplankton cells. In dynamic, high-latitude environments, additional physiological factors, such as internal transport limitations and self-shading Wirtz (2011), which are more important in larger cells but are not considered here, may be more significant.

and nutrient availability in a time-varying, 1-D environment, representative of the oligotrophic Bermuda Atlantic Time Series site (31°50′N, 64°10′W) in the Sargasso Sea. This choice of site also enables a direct comparison with the work of Bruggeman and Kooijman (2007).

Observations indicate that there is significant seasonal variability in the biomass and community structure of phytoplankton at BATS. Small eukaryotic photoautotrophs tend to dominate in terms of carbon biomass during the spring bloom. However, as the water column stratifies coming into the summer, the biomass of *Prochlorococcus* cells rises to nearly equal that of the eukaryotes (DuRand et al. 2001). This transition is indicative of a shift in environmental conditions from (relatively) nutrient-replete conditions during the spring bloom to nutrient-limited conditions during the summer and fall.

Output from the model for surface phosphate, PAR, phytoplankton biomass, the mean population cell size, the mean population investment in the photosynthetic apparatus, and the mean population investment in the biosynthetic apparatus for the final year of a 20 yr simulation at BATS are shown in Fig. 6. Trends in phytoplankton biomass are roughly in keeping with observations, with a peak in biomass during the small spring bloom, followed by a shift to lower biomass in the surface and the formation of a deep chlorophyll maximum at ~ 100 m.

The model reproduces qualitative temporal and spatial observed trends in cell size, with larger cell sizes being positively selected during the initiation of the spring bloom, followed by a shift to small cell size in surface waters and an increase in cell size with depth. This is further illustrated in Fig. 7, which gives an indication of how the agent population is distributed throughout trait space for two depth slices, one taken at 10 m and the other at 100 m.

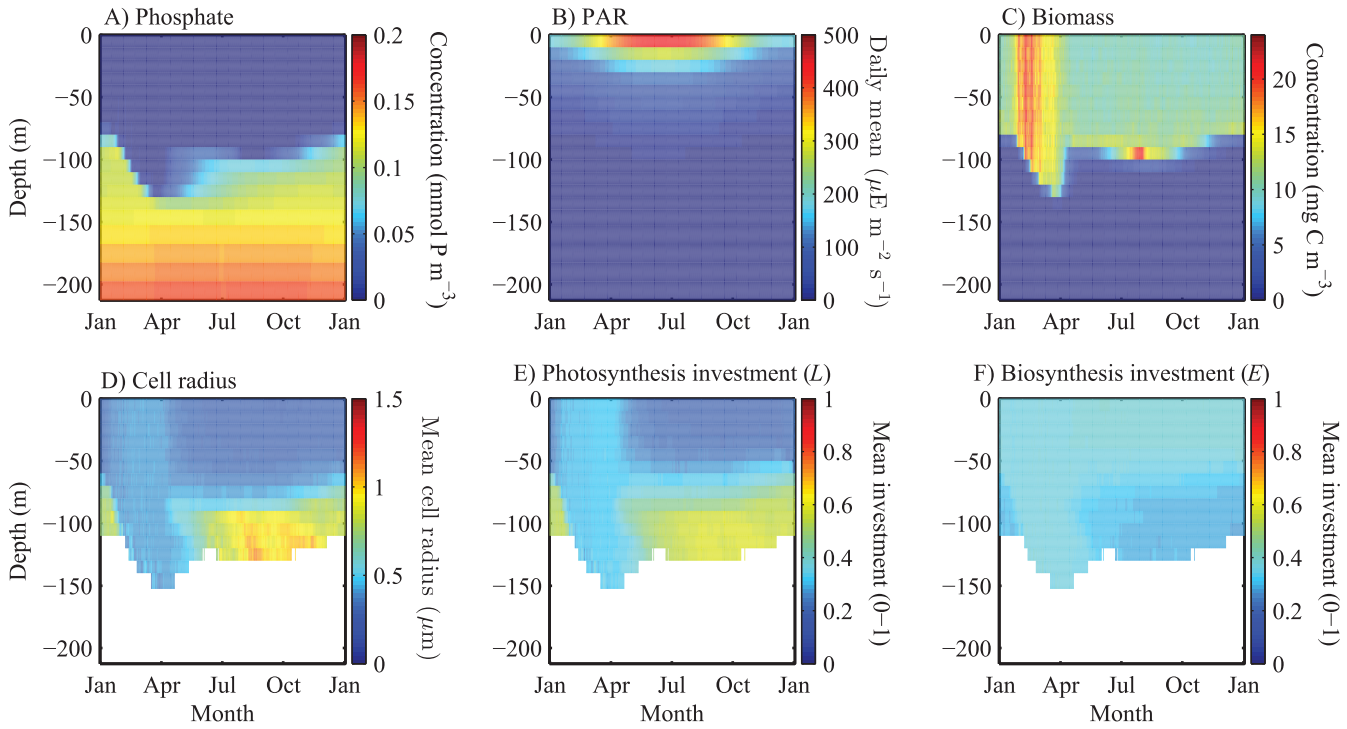

Fig. 6. Model output from the final year of a 20 yr simulation performed at BATS, showing (A) phosphate, (B) PAR, (C) population biomass, (D) the biomass-weighted mean population cell radius, (E) the biomass-weighted mean population investment in the photosynthetic apparatus, and (F) the biomass-weighted mean population investment in the biosynthetic apparatus.

During the months of January, February, and March, covering the spring phytoplankton bloom, the water column is well mixed, and a relatively diverse agent population emerges (Fig. 7A,C). During the months of July, August, and September, the water column is stratified, and a clear split emerges between the two depth slices (Fig. 7B,D). This indicates competitive exclusion—especially evident in surface waters, where cells are smaller and the fitness gradient as a function of cell size is higher—by the smallest cells, which are optimally adapted to their respective local environments.

These results are then consistent with the model of Bruggeman and Kooijman (2007), who observed an increased investment in light-harvesting machinery at depth as the water column restratifies following the spring bloom and a concomitant increased investment in nutrient-harvesting machinery (for which our structural biomass pool acts as a proxy) in surface waters.

Resource competition in stratified environments: During late summer at BATS, the biomass of *Prochlorococcus* cells rises and is comparable to that of small eukaryotes (DuRand et al. 2001), which we take as an indication that conditions are approaching those seen year-round in more extreme oligotrophic environments, where *Prochlorococcus* represents the majority of the autotroph biomass (Hickman et al. 2010; Bouman et al. 2011) and picoeukaryotes meet their nutrient requirements via phagotrophy (Hartmann et al. 2012).

In oligotrophic environments, *Prochlorococcus* ecotype abundances are observed to vary with depth (Zinser et al. 2007; Malmstrom et al. 2010), with high-light–adapted strains, such as eMIT9312 and eMED4, peaking at relatively shallow depths and low-light–adapted strains, such as eSS120 and eMIT9313, having peak abundances at slightly greater depths. This pattern is seen year-round at ALOHA (Malmstrom et al. 2010) and is seen in AMT data (Johnson et al. 2006). As well as adaptations for light level, the *Prochlorococcus* ecotypes also vary by size (Ting et al. 2007), as seen in flow cytometric observations at BATS (DuRand et al. 2001), where mean *Prochlorococcus* cell radii are ~ 0.4 μm at depths $\lessapprox 100$ m in contrast to cell radii of ~ 0.3 μm at the surface.

The 1-D model results (Figs. 6, 7B,D) during late-summer stratification (which we take as an example of behavior year-round in more extreme oligotrophic environments) are consistent with the resource competition argument discussed earlier, with a trend toward increasing cell size with higher nutrient levels but lower light levels at increasing depths. We suggest that this trade-off in the most extreme oligotrophic environments has selected for the trait combinations seen in *Prochlorococcus* ecotypes and that environmental selection based on light level then maintains the observed vertical distribution of ecotypes in less resource limited environments. This would then be responsible for the rapid reestablishment of this pattern as the water column restratifies coming into the summer at BATS, but nutrient levels remain relatively high (Malmstrom et al. 2010).

The model does not reproduce the picoeukaryote population seen in extreme oligotrophic environments, which we attribute to the absence of phagotrophy by picoeukaryotes (Hartmann et al. 2012), missing top-down controls (where size-dependent predation limits the population

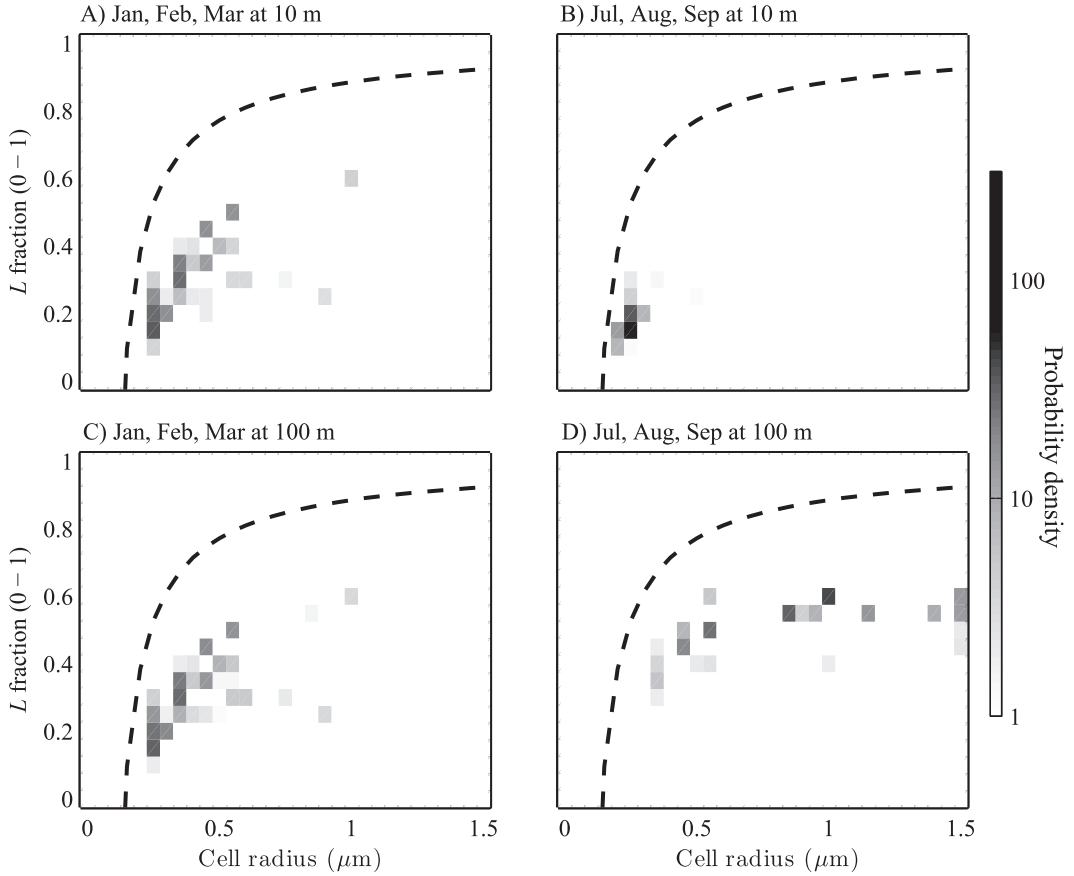

Fig. 7. Time-integrated agent biomasses as a function of cell size and investment in the photosynthetic apparatus normalized against the total biomass. Data are integrated over the months of January, February, and March at depths of (A) 10 m and (C) 100 m and over the months of July, August, and September, also at depths of (B) 10 m and (D) 100 m. The dashed black line in each plot demarcates the limit imposed on allocation to the photosynthetic apparatus as a function of cell size arising from the necessary allocation of resources to structural components.

size of the smallest cells), or missing stochastic mixing (and thus nutrient supply) via mesoscale (McGillicuddy et al. 1998) and submesoscale (Calil and Richards 2010) processes.

Nutrient levels in extreme oligotrophic environments: Given the single-nutrient basis of the model, it is unrealistic to expect detailed agreement with nutrient levels, but a comparison of trends is nevertheless instructive. In the model, surface phosphate concentrations fall to $\sim$ 0.4 nmol L^{-1} during the summer and fall, with values varying between $\sim$ 0.05 and $\sim$ 0.8 nmol L^{-1} over the course of a day (data not shown). Subnanomolar phosphate concentrations have been reported in the ultraoligotrophic South Sargasso Sea (Wu 2000) and in the eastern Mediterranean (Moutin et al. 2002). Other measurements in ultraoligotrophic regions of the North Atlantic gyre have reported concentrations of $\sim$ 2 nmol L^{-1} (Zubkov et al. 2007). These values are somewhat lower than the lowest observed levels at BATS, where data indicate that levels remain at low nanomolar ($<$ 10 nmol L^{-1}) concentrations (Wu 2000), consistent with a scenario where BATS is at the eutrophic limit of the environmental gradient where bottom-up controls dominate.

The discrepancy between observed and modeled levels of phosphate in extreme oligotrophic environments may have multiple causes. Limitation by other nutrients, such as ammonium, or physiological (enzyme) limits on nutrient uptake at very low concentrations, perhaps combined with the preferential utilization of organic phosphorus (Moore et al. 2005; Martiny et al. 2006; Scanlan et al. 2009), would likely limit the minimum observed level of inorganic phosphate. Unresolved top-down controls on the population size of the smallest cells, would also allow nutrient levels to rise. Alternatively, physiological adaptations in response to phosphate limitation, which effectively reduce an organism's quota for phosphate (e.g., via the replacement of phospholipids with sulfolipids (Van Mooy et al. 2009) below the Redfield ratio of 106 : 1 assumed in the model, may also be important.

Discussion

We have investigated the influence of bottom-up controls from light and nutrient limitation and size-dependent trade-offs for the smallest cells, on patterns in phytoplankton biogeography. Our model indicates that extreme small cell size in phytoplankton leads to a trade-off between cell size, nutrient and light affinity, and growth rate, which arises due to the necessary allocation of resources to nonscalable components. The model is

consistent with an apparent decrease in maximum growth rate for the smallest ($\lessapprox 1\ \mu m^3$) cells (Finkel et al. 2010; Wirtz 2011) that has also been attributed to increased metabolite leakage and to maintenance energy requirements in other studies.

The model is qualitatively consistent with overall patterns in phytoplankton biogeography, with seasonally stratified, high-latitude environments being dominated by larger, fast-growing cells, while in stratified, nutrient-supply–limited environments, smaller cells dominate. In stratified environments, the model also reproduces observed trends toward increasing picophytoplankton cell size with increasing depth, which follows from the competitive exclusion of smaller cells with increasing nutrient but decreasing light levels. The model is supported by proteomics data for the smallest cells in extreme oligotrophic environments (Sowell et al. 2009) and evidence for streamlined architectures (Ting et al. 2007). Both of these suggest that our model captures a key scaling of resource allocation with size that directly affects fitness. This is further supported by the direct evidence for a reduction in the maximum growth rate for some of the smallest cells (Bec et al. 2008).

In practice, there remains considerable uncertainty in quantifying resource allocation to ''nonscalable structurally associated'' components, and our model makes numerous simplifying assumptions. In particular, the calculation of cell composition is limited by (1) uncertainties in values, (2) variation between ecotypes, and (3) uncertainty in quantifying less directly cell-surface–associated components. Future studies could further extend our theoretical approach by directly comparing with observed allocations to structural components by different organism types and any concomitant changes in maximum growth rate.

Our ecosystem model for resource competition and trade-offs is directly applicable where the smallest photoautotrophs are dominating the photoautotroph nutrient uptake, that is, the ultraoligotrophic regions described by Zubkov et al. (2007) and Hartmann et al. (2012). Our hypothesis is that *Prochlorococcus* has evolved to be adapted to these environments, with consequent trade-offs in cell size and light acclimation. The regime may extend as a far as periods of summer stratification in less extreme oligotrophic environments, such as BATS. However, beyond these regions, other controls on the phytoplankton cell size distribution are likely to be more important. In future work, our mechanistic, trait-based approach could be extended to include controls on the whole cell size spectrum, with both a physiologically motivated model for larger photoautotrophs, including internal transport limitations for nutrients and light (Wirtz 2011) and additional strategies to mitigate the effects of a decreasing ratio of surface area to volume (Cermeño et al. 2006; Young 2006) acting in combination with a trait-based approach to size-dependent predation (Armstrong 1994).

Our overall approach is based on a mechanistic model of the marine ecosystem that builds on the work of Follows et al. (2007) and Bruggeman and Kooijman (2007). It includes a mechanistic model for interactions between organisms and their environment, a mechanistic model for organism physiology based on subcellular resource allocation, and a model for ecoevolutionary dynamics that represents rapid adaptation of the microbial population. The overall approach is based on the simple initial hypothesis (following Shuter 1979) that phytoplankton strategies can be explained as the adaptive result of resource allocation to evolutionarily conserved (and species-independent) subcellular components (Tilman 1988; 1990; Bruggeman and Kooijman 2007). It may be readily extended to study dynamic acclimation (Geider et al. 1998; Bonachela et al. 2011), the management of storage pools (Ross and Geider 2009; Wirtz and Pahlow 2010), and ecotype-dependent aspects of organism physiology (e.g., in pigment composition; Hickman et al. 2010).

By representing selection in a dynamic, ecological environment, our approach essentially generalizes the application of optimality principles (Parker and Smith 1990; Smith et al. 2011) and cost–benefit arguments (Raven 1984). Such a mechanistic and physiologically motivated approach has several potential advantages (e.g., *see* discussion by Follows and Dutkiewicz 2011) over other approaches to modeling the marine ecosystem. First, it provides a parameter-sparse representation of microbial diversity based on a model for organism physiology and traits rather than empirical measurements of organism properties (Le Quéré et al. 2005). Second, the mechanistic basis allows model tests against data that highlight missing processes (as here) rather than considering data comparisons as a mechanism for parameter estimation, as may be the case in highly aggregated (e.g., nutrient–phytoplankton–zooplankton–detritus) models. Finally, the coarse-grained representation of cellular physiology provides a link to more detailed systems-biology approaches (Buescher et al. 2012) and to omics data sets (Gilbert et al. 2011). Ultimately, such mechanistic approaches may help us understand the likely response of the marine ecosystem to global change.

Acknowledgments

We thank two anonymous reviewers for their careful reading of the manuscript and constructive criticism. We thank Stephanie Dutkiewicz and Anna Hickman, who provided help with running and configuring the Massachusetts Institute of Technology Ocean General Circulation Model. The calculations for this article were performed using the University of Exeter Supercomputer. J.C. and S.D. were supported by the Leverhulme Trust (F/00 204/AP).

References

Adcroft, A., S. Dutkiewicz, D. Ferreira, P. Heimbach, O. Jahn, and G. Maze. 2011. MITgcm user manual. Available from http://mitgcm.org

Anderson, T. R. 2005. Plankton functional type modelling: Running before we can walk? J. Plankton Res. **27:** 1073–1081.

Armstrong, R. A. 1994. Grazing limitation and nutrient limitation in marine ecosystems: Steady state solutions of an ecosystem model with multiple food chains. Limnol. Oceanogr. **39:** 597–608, doi:10.4319/lo.1994.39.3.0597

Baas-Becking, L. G. M. 1934. Geobiologie of inleiding tot de milieukunde. W. P. van Stockum and Zoon N. V. [Geobiology or introduction to the science of the environment.]

Barton, A. D., S. Dutkiewicz, G. Flierl, J. Bragg, and M. J. Follows. 2010. Patterns of diversity in marine phytoplankton. Science **327:** 1509–1511, doi:10.1126/science.1184961

Bec, B., Y. Collos, A. Vaquer, D. Mouillot, and P. Souchu. 2008. Growth rate peaks at intermediate cell size in marine photosynthetic picoeukaryotes. Limnol. Oceanogr. **53:** 863–867, doi:10.4319/lo.2008.53.2.0863

Berg, H. C., and E. M. Purcell. 1977. Physics of chemoreception. Biophys. J. **20:** 193–219, doi:10.1016/S0006-3495(77)85544-6

Bloom, A. J., F. S. Chapin, III, and H. A. Mooney. 1985. Resource limitation in plants—an economic analogy. Annu. Rev. Ecol. Syst. **16:** 363–392.

Bonachela, J. A., M. Raghib, and S. A. Levin. 2011. Dynamic model of flexible phytoplankton nutrient uptake. Proc. Natl. Acad. Sci. USA **108:** 20633–20638, doi:10.1073/pnas.1118012108

Bouman, H. A., and others. 2011. Water-column stratification governs the community structure of subtropical marine picophytoplankton. Environ. Microbiol. Rep. **3:** 473–482, doi:10.1111/j.1758-2229.2011.00241.x

Bruggeman, J., and S.A.L.M. Kooijman. 2007. A biodiversity-inspired approach to aquatic ecosystem modeling. Limnol. Oceanogr. **52:** 1533–1544, doi:10.4319/lo.2007.52.4.1533

Buescher, J. M., and others. 2012. Global network reorganization during dynamic adaptations of *Bacillus subtilis* metabolism. Science **335:** 1099–1103, doi:10.1126/science.1206871

Calil, P. H. R., and K. J. Richards. 2010. Transient upwelling hot spots in the oligotrophic North Pacific. J. Geophys. Res. **115:** C02003, doi:10.1029/2009JC005360

Cermeño, P., E. Marañón, D. Harbour, and R. P. Harris. 2006. Invariant scaling of phytoplankton abundance and cell size in contrasting marine environments. Ecol. Lett. **9:** 1210–1215, doi:10.1111/j.1461-0248.2006.00973.x

Chisholm, S. 1992. Phytoplankton size, p. 213–237. *In* P. G. Falkowski and A. D. Woodhead [eds.], Primary productivity and biogeochemical cycles in the sea. Plenum Press.

Clark, J. R., S. J. Daines, T. M. Lenton, A. J. Watson, and H. Williams. 2011. Individual-based modelling of adaptation in marine microbial populations using genetically defined physiological parameters. Ecol. Model. **222:** 3823–3837, doi:10.1016/j.ecolmodel.2011.10.001

Courties, C., and others. 1994. Smallest eukaryotic organism. Nature **370:** 255, doi:10.1038/370255a0

Dufresne, A., L. Garczarek, and F. Partensky. 2005. Accelerated evolution associated with genome reduction in a free-living prokaryote. Genome Biol. **6:** R14, doi:10.1186/gb-2005-6-2-r14

DuRand, M., R. Olson, and S. Chisholm. 2001. Phytoplankton population dynamics at the Bermuda Atlantic time-series station in the Sargasso Sea. Deep-Sea Res. II **48:** 1983–2003, doi:10.1016/S0967-0645(00)00166-1

Dutkiewicz, S., M. J. Follows, and J. G. Bragg. 2009. Modeling the coupling of ocean ecology and biogeochemistry. Glob. Biogeochem. Cycles **23:** GB4017, doi:10.1029/2008GB003405

Fasham, M. J. R., H. W. Ducklow, and S. M. McKelvie. 1990. A nitrogen-based model of plankton dynamics in the oceanic mixed layer. J. Mar. Res. **48:** 591–639.

Finkel, Z. V., J. Beardall, K. J. Flynn, A. Quigg, T. A. V. Rees, and J. A. Raven. 2010. Phytoplankton in a changing world: Cell size and elemental stoichiometry. J. Plankton Res. **32:** 119–137, doi:10.1093/plankt/fbp098

Flynn, K. J. 2006. Reply to Horizons Article "Plankton functional type modelling: Running before we can walk" Anderson (2005): II. Putting trophic functionality into plankton functional types. J. Plankton Res. **28:** 873–875, doi:10.1093/plankt/fbl015

Follows, M. J., and S. Dutkiewicz. 2011. Modeling diverse communities of marine microbes. Annu. Rev. Mar. Sci. **3:** 427–451, doi:10.1146/annurev-marine-120709-142848

———, ———, S. Grant, and S. W. Chisholm. 2007. Emergent biogeography of microbial communities in a model ocean. Science **315:** 1843–1846, doi:10.1126/science.1138544

Garcia, H. E., R. A. Locarnini, T. P. Boyer, and J. I. Antonov. 2006. World ocean atlas 2005. Volume 4: Nutrients (phosphate, nitrate, silicate), S. Levitus [ed.], NOAA Atlas NESDIS 64. U.S. Government Printing Office.

Geider, R. J., H. L. MacIntyre, and T. M. Kana. 1996. A dynamic model of photoadaptation in phytoplankton. Limnol. Oceanogr. **41:** 1–15, doi:10.4319/lo.1996.41.1.0001

———, ———, and ———. 1997. Dynamic model of phytoplankton growth and acclimation: Responses of the balanced growth rate and the chlorophyll *a*:carbon ratio to light, nutrient-limitation and temperature. Mar. Ecol. Prog. Ser. **148:** 187–200, doi:10.3354/meps148187

———, ———, and ———. 1998. A dynamic regulatory model of phyto-planktonic acclimation to light, nutrients, and temperature. Limnol. Oceanogr. **43:** 679–694, doi:10.4319/lo.1998.43.4.0679

———, C. M. Moore, and O. N. Ross. 2009. The role of cost-benefit analysis in models of phytoplankton growth and acclimation. Plant Ecol. Divers. **2:** 165–178, doi:10.1080/17550870903300949

Gent, P. R., and J. C. McWilliams. 1990. Isopycnal mixing in ocean circulation models. J. Phys. Oceanogr. **20:** 150–155, doi:10.1175/1520-0485(1990)020<0150:IMIOCM>2.0.CO;2

Gilbert, J. A., and others. 2011. Defining seasonal marine microbial community dynamics. ISME J. **6:** 298–308, doi:10.1038/ismej.2011.107

Giovannoni, S. J., and others. 2005. Genome streamlining in a cosmopolitan oceanic bacterium. Science **309:** 1242–1245, doi:10.1126/science.1114057

Hartmann, M., C. Grob, G. A. Tarran, A. P. Martin, P. H. Burkill, D. J. Scanlan, and M. V. Zubkov. 2012. Mixotrophic basis of Atlantic oligotrophic ecosystems. Proc. Natl. Acad. Sci. USA **109:** 5756–5760, doi:10.1073/pnas.1118179109

Hellweger, F. L., and E. Kianirad. 2007. Individual-based modeling of phytoplankton: Evaluating approaches for applying the cell quota model. J. Theor. Biol. **249:** 554–565, doi:10.1016/j.jtbi.2007.08.020

Hickman, A. E., S. Dutkiewicz, R. G. Williams, and M. J. Follows. 2010. Modelling the effects of chromatic adaptation on phytoplankton community structure in the oligotrophic ocean. Mar. Ecol. Prog. Ser. **406:** 1–17, doi:10.3354/meps08588

Irwin, A. J., Z. E. Finkel, O. M. E. Schofield, and P. G. Falkowski. 2006. Scaling-up from nutrient physiology to the size-structure of phytoplankton communities. J. Plankton Res. **28:** 459–471, doi:10.1093/plankt/fbi148

Jiang, S., P. H. Stone, and P. Malanotte-Rizzoli. 1999. An assessment of the Geophysical Fluid Dynamics Laboratory ocean model with coarse resolution: Annual-mean climatology. J. Geophys. Res. **25:** 623–625.

Johnson, Z. I., E. Zinser, A. Coe, N. P. McNulty, E. M. S. Woodward, and S. W. Chisholm. 2006. Niche partitioning among *Prochlorococcus* ecotypes along ocean-scale environmental gradients. Science **311:** 1737–1740, doi:10.1126/science.1118052

Karl, D. M., and others. 2003. Temporal studies of biogeochemical processes determined from ocean time-series observations during the JGOFS era, p. 239–267. *In* M. J. R. Fasham [ed.], Ocean biogeochemistry: The role of the ocean carbon cycle in global change (a JGOFS Synthesis). Springer.

Kiørboe, T. 2008. A mechanistic approach to plankton ecology. Princeton University Press.

Kooijman, S.A.L.M. 2000. Dynamic energy and mass budgets in biological systems. Cambridge University Press.

Large, W., J. McWilliams, and S. C. Doney. 1994. Oceanic vertical mixing: A review and a model with a nonlocal boundary layer parameterization. Rev. Geophys. **32:** 363–403, doi:10.1029/94RG01872

Le Quéré, C. L., and others. 2005. Ecosystem dynamics based on plankton functional types for global ocean biogeochemistry models. Glob. Change Biol. **11:** 2016–2040.

Levitus, S., and T. P. Boyer. 1994*a*. World ocean atlas 1994. Volume 3: Salinity. Technical report. NOAA Atlas NESDID 3.

———, and ———. 1994*b*. World ocean atlas 1994. Volume 4: Temperature. Technical report. NOAA Atlas NESDID 4.

Locarnini, R. A., A. V. Mishonov, J. I. Antonov, T. P. Boyer, and H. E. Garcia. 2006. World ocean atlas 2005, Volume 1: Temperature, S. Levitus [ed.], NOAA Atlas NESDIS 61. U.S. Government Printing Office.

Madigan, M. T., and J. M. Martinko. 2009. Brock biology of microorganisms. Pearson Prentice Hall.

Malmstrom, R. R., A. Coe, G. C. Kettler, A. C. Martiny, J. Frias-Lopez, E. Zinser, and S. W. Chisholm. 2010. Temporal dynamics of *Prochlorococcus* ecotypes in the Atlantic and Pacific oceans. ISME J. **4:** 1252–1264, doi:10.1038/ismej.2010.60

Martiny, A. C., M. L. Coleman, and S. W. Chisholm. 2006. Phosphate acquisition genes in *Prochlorococcus* ecotypes: Evidence for genome-wide adaptation. Proc. Natl. Acad. Sci. USA **103:** 12552–12557, doi:10.1073/pnas.0601301103

McGillicuddy, D., A. Robinson, and D. Siegel. 1998. Influence of mesoscale eddies on new production in the Sargasso Sea. Nature **285:** 263–266, doi:10.1038/28367

Mei, Z.-P., Z. V. Finkel, and A. Irwin. 2009. Light and nutrient availability affect the size-scaling of growth in phytoplankton. J. Theor. Biol. **259:** 582–588, doi:10.1016/j.jtbi.2009.04.018

Moore, L., M. Ostrowski, D. Scanlan, K. Feren, and T. Sweetsir. 2005. Ecotypic variation in phosphorus-acquisition mechanisms within marine picocyanobacteria. Aquat. Microb. Ecol. **39:** 257–269, doi:10.3354/ame039257

Morel, A., Y.-H. Ahn, F. Partensky, D. Vaulot, and H. Claustre. 1993. *Prochlorococcus* and *Synechococcus*: A comparative study of their optical properties in relation to their size and pigmentation. J. Mar. Res. **51:** 617–649, doi:10.1357/0022240933223963

Moutin, T., T. F. Thingstad, F. V. Wambeke, D. Marie, P. Raimbault, and H. Claustre. 2002. Does competition for nanomolar phosphate supply explain the predominance of the cyanobacterium *Synechococcus*? Limnol. Oceanogr. **47:** 1562–1567, doi:10.4319/lo.2002.47.5.1562

Muddiman, D. C., G. A. Anderson, S. A. Hofstadler, and R. D. Smith. 1997. Length and base composition of PCR-amplified nucleic acids using mass measurements from electrospray ionization mass spectrometry. Anal. Chem. **69:** 1543–1549, doi:10.1021/ac961134r

Neidhardt, F. C., J. L. Ingraham, and M. Schaechter. 1990. Physiology of the bacterial cell: A molecular approach. Sinauer Associates Inc.

Nicastro, D., C. Schwartz, J. Pierson, J.-C. Cho, S. J. Giovannoni, and J. R. McIntosh. 2006. Three-dimensional structure of the tiny bacterium *Pelagibacter ubique* studied by cryo-electron tomography. Microsc. Microanal. **12:** 180–181, doi:10.1017/S1431927606067456

Parker, G. A., and J. M. Smith. 1990. Optimality theory in evolutionary biology. Nature **348:** 27–33, doi:10.1038/348027a0

Partensky, F., and L. Garczarek. 2010. *Prochlorococcus*: Advantages and limits of minimalism. Annu. Rev. Mar. Sci. **2:** 305–331, doi:10.1146/annurev-marine-120308-081034

Pasciak, W. 1974. Transport limitation of nutrient uptake in phytoplankton. Limnol. Oceanogr. **19:** 881–888, doi:10.4319/lo.1974.19.6.0881

Penning De Vries, F. W. T., A. H. M. Brunsting, and H. H. Van Laar. 1974. Products, requirements and efficiency of biosynthesis: A quantitative approach. J. Theor. Biol. **45:** 339–377, doi:10.1016/0022-5193(74)90119-2

Raven, J. A. 1984. A cost-benefit analysis of photon absorption by photosynthetic unicells. New Phytol. **98:** 593–625, doi:10.1111/j.1469-8137.1984.tb04152.x

———. 1994. Why are there no picoplanktonic O_2 evolvers with volumes less than 10^{-19} m^3? J. Plankton Res. **16:** 565–580, doi:10.1093/plankt/16.5.565

———. 1999. Picophytoplankton. Prog. Phycol. Res. **13:** 33–106.

———, Z. V. Finkel, and A. Irwin. 2005. Picophytoplankton: Bottom-up and top-down controls on ecology and evolution. Vie Milieu **55:** 209–215.

Reynolds, C. S. 2006. The ecology of phytoplankton. Cambridge University Press.

Rose, K. 1993. Individual-based modeling of populations with high mortality: A new method based on following a fixed number of model individuals. Ecol. Model. **68:** 273–292, doi:10.1016/0304-3800(93)90022-K

Ross, O. N., and R. J. Geider. 2009. New cell-based model of photosynthesis and photo-acclimation: Accumulation and mobilisation of energy reserves in phytoplankton. Mar. Ecol. Prog. Ser. **383:** 53–71, doi:10.3354/meps07961

Scanlan, D. J., and others. 2009. Ecological genomics of marine picocyanobacteria. Microbiol. Mol. Biol. Rev. **73:** 249–99, doi:10.1128/MMBR.00035-08

Scheffer, M., J. M. Baveco, D. L. DeAngelis, K. A. Rose, and E. H. van Nes. 1995. Superindividuals a simple solution for modeling large populations on an individual basis. Ecol. Model. **80:** 161–170, doi:10.1016/0304-3800(94)00055-M

Shuter, B. J. 1979. A model of physiological adaptation in unicellular algae. J. Theor. Biol. **78:** 519–552, doi:10.1016/0022-5193(79)90189-9

Smith, S. L., M. Pahlow, A. Merico, and K. W. Wirtz. 2011. Optimality-based modeling of planktonic organisms. Limnol. Oceanogr. **56:** 2080–2094, doi:10.4319/lo.2011.56.6.2080

Sowell, S. M., and others. 2009. Transport functions dominate the SAR11 metaproteome at low-nutrient extremes in the Sargasso Sea. ISME J. **3:** 93–105, doi:10.1038/ismej.2008.83

Steinberg, D., C. Carlson, N. Bates, R. Johnson, A. Michaels, and A. Knap. 2001. Overview of the US JGOFS Bermuda Atlantic time-series study (BATS): A decade-scale look at ocean biology and biogeochemistry. Deep-Sea Res. II **48:** 1405–1447, doi:10.1016/S0967-0645(00)00148-X

Tambi, H., G. Flaten, J. K. Egge, G. Bødtker, A. Jacobsen, and T. F. Thingstad. 2009. Relationship between phosphate affinities and cell size and shape in various bacteria and phytoplankton. Aquat. Microb. Ecol. **57:** 311–320, doi:10.3354/ame01369

Thingstad, T. F., E. Strand, and A. Larsen. 2010. Stepwise building of plankton functional type (PFT) models: A feasible route to complex models? Prog. Oceanogr. **84:** 6–15, doi:10.1016/j.pocean.2009.09.001

Tilman, D. 1982. Resource competition and community structure. Princeton University Press.

———. 1988. Plant strategies and the dynamics and structure of plant communities. Princeton University Press.

———. 1990. Constraints and tradeoffs: Toward a predictive theory of competition and succession. Oikos **58:** 3–15, doi:10.2307/3565355

Ting, C. S., C. Hsieh, S. Sundararaman, C. Mannella, and M. Marko. 2007. Cryo-electron tomography reveals the comparative three-dimensional architecture of *Prochlorococcus*, a globally important marine cyanobacterium. J. Bacteriol. **189:** 4485–4493, doi:10.1128/JB.01948-06

Trenberth, K., W. Large, and J. Olson. 1989. A global ocean wind stress climatology based on ECMWF analyses. TN-338+STR. Technical report. National Center for Atmospheric Research.

Van Mooy, B. A. S., and others. 2009. Phytoplankton in the ocean use non-phosphorus lipids in response to phosphorus scarcity. Nature **458:** 69–72, doi:10.1038/nature07659

Williams, R. G., and M. J. Follows. 1998. The Ekman transfer of nutrients and maintenance of new production over the North Atlantic. Deep-Sea Res. I **45:** 461–489, doi:10.1016/S0967-0637(97)00094-0

———, and ———. 2003. Physical transport of nutrients and the maintenance of biological production, chap. 2. *In* M. Fasham [ed.], Ocean biogeochemistry: The role of the ocean carbon cycle in global change (a JGOFS Synthesis). Springer.

Wirtz, K. W. 2011. Non-uniform scaling in phytoplankton growth rate due to intracellular light and CO2 decline. J. Plankton Res. **33:** 1325–1341, doi:10.1093/plankt/fbr021

———, and M. Pahlow. 2010. Dynamic chlorophyll and nitrogen:carbon regulation in algae optimizes instantaneous growth rate. Mar. Ecol. Prog. Ser. **402:** 81–96, doi:10.3354/meps08333

Woods, J., A. Perilli, and W. Barkmann. 2005. Stability and predictability of a virtual plankton ecosystem created with an individual-based model. Prog. Oceanogr. **67:** 43–83, doi:10.1016/j.pocean.2005.04.004

Wu, J. 2000. Phosphate depletion in the western North Atlantic Ocean. Science **289:** 759–762, doi:10.1126/science.289.5480.759

Young, K. D. 2006. The selective value of bacterial shape. Microbiol. Mol. Biol. Rev. **70:** 660–703, doi:10.1128/MMBR.00001-06

Zinser, E., Z. Johnson, A. Coe, E. Karaca, D. Veneziano, and S. Chisholm. 2007. Influence of light and temperature on *Prochlorococcus* ecotype distributions in the Atlantic Ocean. Limnol. Oceanogr. **52:** 2205–2220, doi:10.4319/lo.2007.52.5.2205

Zubkov, M. V., and others. 2007. Microbial control of phosphate in the nutrient-depleted North Atlantic subtropical gyre. Environ. Microbiol **9:** 2079–2089, doi:10.1111/j.1462-2920.2007.01324.x

Associate editor: Heidi M. Sosik

Received: 09 May 2012
Accepted: 22 January 2013
Amended: 06 February 2013